IEEE Access
Multidisciplinary | Rapid Review | Open Access Journal

Received June 20, 2019, accepted July 8, 2019, date of publication July 19, 2019, date of current version August 7, 2019.

Digital Object Identifier 10.1109/ACCESS.2019.2929946

Development and Application of a Reconfigurable Photovoltaic Inverter for Operation Within a Microgrid

RUBÉN ORTEGA[1,2], OSCAR CARRANZA[1,2], (Member, IEEE), JAIME JOSÉ RODRÍGUEZ[2], (Member, IEEE), VÍCTOR H. GARCÍA[1], JULIO C. SOSA[3], AND JOSÉ M. ALVARADO[2]

[1]Instituto Politécnico Nacional, Escuela Superior de Cómputo, Ciudad de México 07838, México
[2]Instituto Politécnico Nacional, Escuela Superior de Ingeniería Mecánica y Eléctrica, Ciudad de México 07738, México
[3]Instituto Politécnico Nacional, Centro de Investigación en Ciencia Aplicada y Tecnología Avanzada, Querétaro 76090, México

Corresponding author: Rubén Ortega (rortegag@ipn.mx)

This work was financial supported for publication by the Comisión de Operación y Fomento de Actividades Académicas del Instituto Politécnico Nacional.

ABSTRACT Smart grids have their basis in distribution systems, and to take advantage of their full potential, the incorporation of distributed generation must be taken into account. This new strategy allows the decentralization of power generation and the microgrid represents a very important element in this generation scheme. With this perspective and considering the importance of power converters, this paper presents the development and operation of a reconfigurable photovoltaic inverter; which aims to operate in grid-connected mode and disconnected from this. To achieve this goal, a hierarchical control is proposed that serves as the basis to develop controllers at level one and level two. Particularly, in grid-disconnected operation, in level one of the hierarchical control a droop controller is implemented whose objective is to give the reference to be followed by the voltage loop controller; as well as allow that between inverters parallel connected, these can be distributed the active and reactive power demanded by the load. In level two of the hierarchical control, the controllers of the current and voltage loops are implemented for both modes of operation. Particularly, in grid-disconnected operation, the following contributions are made to this work: an integral sliding mode controller is implemented; which is a novelty for this application. The goal of this controller is to reduce the total harmonic distortion of the voltage signal that is delivered to the local load in this operation mode. Also, it presents a good performance at the moment of the transition of grid-disconnected operation to the connected operation to this. In addition, a synchronization algorithm was implemented for the inverter reconnection with the grid, as well as an algorithm for the detection of islanding.

INDEX TERMS Photovoltaic inverter, reconfigurable, hierarchical control, integral sliding mode control scheme, droop scheme, microgrid.

I. INTRODUCTION

The current electrical systems are in an important stage of transformation being aspects such as economic, technological and environmental, factors that motivate a change towards new strategies of generation and transmission of energy throughout the world.

The existing generation and distribution systems have to change to adapt to the new generation strategies based on distributed generation, allowing greater autonomy and system flexibility. Characteristics such as; guarantee the system reliability, have the ability to adapt to the management of renewable energy and present increases in the generation efficiency are basic objectives of a distribution system based on distributed generation.

Smart grids have their main component in distribution systems, and in order to take full advantage of their potential as part of the future grid, through the incorporation of distributed generation, it is necessary to decentralize their structure [1], [2]. The new paradigm that allows this

The associate editor coordinating the review of this manuscript and approving it for publication was Shuo Sun.

decentralization is the microgrid, which can be considered as one of the fundamental elements of the new smart grid model [3]–[5].

A microgrid, is a secondary grid that operates at the level of energy distribution and its main characteristic is to be able to operate both grid-interconnected and disconnected from this. To have this generation capacity the microgrid has local generation typically in the form of distributed generation that allows it to function as an electric island under different situations, both desired and unwanted.

Microgrids are a useful tool for both rural and urban areas, as well as for developed and developing countries, despite representing very different realities. In the case of rural areas, or developing economies, a microgrid *ac* be a very good electrification alternative that, for example, supplies electricity for the first time to a remote location (continuously operating in island mode). If in the future it is possible to have a grid connection point, the microgrid will be able to work interconnected to this. Under this scheme, control systems and energy storage systems will allow the management of energy obtained through renewable energy sources, which leads to a more sustainable development of the community [6]–[9].

Considering the importance of microgrids in the new generation strategies, based on renewable energy, different research projects have been developed; where they are analyzed and proposed solutions for their correct operation, for example in: [10] a novel control structure is proposed for the single phase inverter either operating in grid connecting mode or in islanding mode. The system is designed in such a way that the same control structure can work both in grid connected and in islanding mode without islanding detection. In [11] it is analyzed the problem of the distributed generation technology to realize the seamless switching between the grid and the island operating modes and reduce the current and voltage impulse. In [12] is presents a seamless transition method for droop-controlled inverters to operate in both islanding and grid-connected modes. A local PLL and a virtual inductance are designed to ride through transient when the inverter switches between two modes without synchronization. The proposed method can cooperatively work with well-developed droop controls so that the inverters are able to share load among them as well as subsist under transient events of the utility. In [13] the transition of a microgrid is confirmed, from the island mode to grid-mode connection, where the synchronization of the microgrid is a very important factor. In this study, a first order low pass filter is replaced by a sliding filter based on the Goertzel transformation; In addition, a control strategy with an extended phase lock loop for inverter applications in island microgrids is presented. This allows to guarantee the synchronization between the voltage signal of the microgrid and the voltage signal of the grid, and to guarantee the perfect grid-reconnection. In [14] a distributed hierarchical control is proposed for ac microgrid, which could apply to both grid-connected (GC) mode and islanded (IS) mode as well as mode transitions. Under the proposed control framework, the following targets are achieved: 1) the frequency/voltage recovery and accurate power sharing in IS mode; 2) flexible power flow regulation between utility-grid and microgrid in *GC* mode; 3) universal control strategy from GC to IS modes without control switching; and 4) smooth active-synchronization from *IS* mode to *GC* mode.

Considering the works described above and analyzing their contributions, this paper develops a proposal for a reconfigurable energy conversion system; where the different elements that allow the integration of this system to a microgrid are described and developed. Starting with the design of a *dc-dc* converter that aims to adapt the energy obtained by means of a renewable energy source (solar) through a panel arrangement; so that it can be converted to *ac* by means of a single-phase inverter. To achieve this, it is implemented through programming: algorithms of maximum power point tracking (MPPT) as well as phase-locked loop (PLL) that allow to maximize the energy obtained by the arrangement of solar panels and the synchronization of inverters with the grid respectively. Islanding detection algorithms and droop schemes are also implemented, which allow the disconnection of converters from the grid for security reasons; as well as their parallel interconnection. Finally, an integral sliding mode control is designed in order to reduce the THDv in grid-disconnected operation.

For the implementation and correct operation of the control schemes and developed algorithms for this application, a four-level hierarchical control system is used that is described in [15].

The primary control [16], [17] is implemented in each power conversion unit connected to the microgrid, being one of the most important, the droop scheme or ''droop control'' [18]. Droop control is a control strategy commonly applied to generators for primary frequency control and sometimes for voltage control; besides allowing the operation of the generator in parallel to share the load.

The secondary control [19]–[21] in a microgrid is called the energy management system (EMS), this type of control is implemented specifically for the grid-interconnected operation and disconnected from this. Allowing, grid-interconnected and disconnected from it to set voltages and frequency references; as well as compensate voltage and frequency deviation. It also allows calculating the restoration factor for voltage and frequency of each inverter, starting from the references established by the tertiary control. It also allows the synchronization of the microgrid with the main grid, balances the tension before unbalance and intervenes in the harmonic compensation.

The tertiary control [22]–[24], allows establishing the references of voltage and frequency for the secondary control of each inverter according to the references established by the tertiary control. This as consequence of the active and reactive power control, which is presented in the main grid and each output of the converter and the references received from the quaternary control.

Finally, the quaternary control performs the management of the entire microgrid, allowing its optimum point of operation, forecasting the demand, energy storage, economic management of the generation systems, always favoring the use of renewable energies [25], [26].

This paper presets the development and operation of reconfigurable photovoltaic inverter to work autonomously in grid-interconnected or disconnected from this. Particularly, a single-phase inverter topology is proposed which, in grid-interconnected mode, works as a current source in phase with the voltage of the electrical grid, injecting power into this. In addition, it is proposed to inverters configure so that it can also operate: in grid-connected mode or grid-disconnected for which it must operate as a voltage source feeding local load.

The contribution of his work focuses on the development and application of controller within the hierarchical scheme described above at the primary and secondary levels. That is, for the primary control of the microgrid, controllers are used under resistive droop schemes, as well as controller for grid-interconnected operation and grid-disconnected operation, which allow to regulate current and voltage respectively. For the secondary control, a new control structure based on an integral sliding mode controller [27] was implemented, which aims to reduce the total harmonic distortion of the voltage signal (THDv) that is delivered to a local load. As well as avoiding excessive transients at the time of the transition from grid-interconnected mode to grid-disconnected mode and from grid-disconnected mode to grid-interconnected mode respectively. In addition, algorithms were implemented for the inverter synchronization with the grid as well as for the detection of islanding.

To validate the system performance, results are presented by means of simulation and experimental tests of the interconnection of two inverter in parallel and their grid-connection, as well as their parallel interconnection for grid-disconnected operation. In addition, signal waveforms obtained by means of simulations and experimental tests are presented during the transitions from grid mode to island mode and from island mode to grid mode.

In addition, waveforms are reported thought simulation of the *dc-dc* converter that validate their performance together with the controller implemented for both conversion systems.

Finally, the performance of the inverter is validated through experimental tests, particularly the inverter reconfiguration and the parallel connection of two inverters. With which it is concluded that the controllers designed for this application have a good performance.

This work is organized as follows: the second section presents the development of the Boost converter and the inverter for grid-connected operation; as well as the agorhythm of island detection. Section three shows the development of the Boost converter and the inverter for grid-disconnected operation, as well as the droop scheme used for the parallel connection of inverters; the integral sliding mode control is also designed for this operation mode. In section four, the results obtained from the converter are presented by means of simulations for both operation modes. In section five, results are presented by means of experimental tests. Finally, in section six the conclusions of the work are presented.

The development of the inverter for its grid-connected operation is described below.

II. INVERTER CONFIGURATION FOR GRID-CONNECTED OPERATION

There are different topologies to perform the energy conversion from a renewable source such as solar energy, and these are: centralized inverter, inverter by association series of panels, as well as inverter by panel or microinverter [28]–[29]. Particularly, this work uses a topology based on the serial connection of solar panels, which is described below.

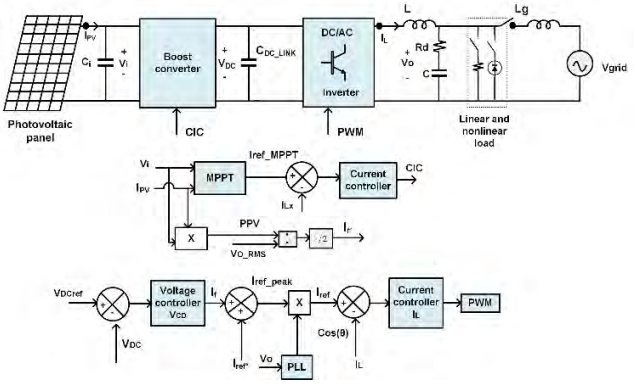

FIGURE 1. Inverter block diagram in the grid-connected operation.

Fig. 1 shows the scheme of the photovoltaic inverter (PV) that was implemented in the grid-connection mode. In this operating mode, the converter is fed by a *dc* source, where the I-V curve of a photovoltaic panel is characterized to emulate a real operation of the photovoltaic panel. The voltage in the panel is 96 V at the maximum power point (MPP), therefore, it is necessary to raise the voltage obtained from the solar panels to a value of 400 V for inverter grid connection; to achieve this goal a *cd-cd* converter is used. In particular, for this application, two 48 V photovoltaic panels will be connected in series.

For the conversion from *dc* to *ac*, an inverter with bridge topology H is used, controlled by current and with pulse width modulation (PWM) [30]. In addition, an LCL filter is used at the output of the converter [31], [32].

The following describes the importance of the use of a phase locked loop for the inverter grid connection, as well as the parameters of its design for this application.

A. PHASE-LOCKED LOOP

The energy obtained by the inverter is injected into the grid when it acts as a current source and is grid-synchronized. To fulfill this objective, it is necessary that the inverter current control is grid-synchronized; which is achieved with the use of a phase-locked loop (PLL) [33], [34] that generally has

applications in three-phase systems, since it bases its operation on a synchronous reference frame (SRF) [35]. However, for single-phase systems the application of an SRF is not possible directly, so it is necessary to generate a quadrature component with the voltage signal in order to apply Park inverse transform [36].

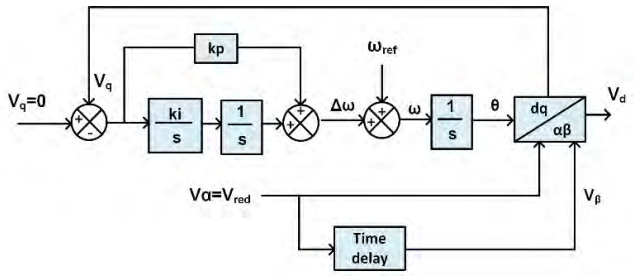

FIGURE 2. Single-phase PLL Algorithm based on the use of a delay to generate the quadrature signal.

To generate this component, a delay is implemented whose purpose is to introduce a displacement of the phase of 90^o with respect to the fundamental frequency of the reference signal. The PLL algorithm that is based on a delay to generate the quadrature signal is shown in Fig. 2. In this scheme, the delay allows to generate a phase shift of 90^o and can be implemented by means of a low pass filter at a cutoff frequency much lower than the frequency of the grid, which in our case is 50 Hz. In particular, the cutoff frequency was set to 5 Hz. The gain of this filter was chosen as a function of the attenuation given by it, particularly it is desired that the signal $V\alpha$ and V_β are equal, obtaining a value of 12Hz.

Once the converter is in grid-interconnected, it is necessary to use a maximum power point tracking (MPPT) algorithm to maximize the power obtained by the panels array. This algorithm is described below

B. MAXIMUM POWER POINT TRACKING (MPPT) OF THE PHOTOVOLTAIC PANEL

Under this generation scheme the amount of energy that can be injected into the grid is determined by the maximum power that can be extracted from the group of photovoltaic panels; this is achieved with the implementation of a maximum power point tracking algorithm (MPPT). There are different techniques for MPPT algorithm, which are based on finding the voltage and current for which the panel or the arrangement of panels allows us to obtain maximum power. However, particularly in this work the technique of perturb and observe is used (P & O) [37].

This algorithm is based on the periodic disturbance that is, increasing or decreasing the voltage at terminals of the array of panels, which is later compared with their output power when considering the disturbance of the previous cycle. Therefore, if the voltage in the connection terminals of the panels array changes and the power increases, the control system regulates the operation point of the array in that direction, otherwise the operation point is located in the opposite direction, presenting this process in an iterative way. The operation frequency of the MPPT algorithm that has been chosen is 50 Hz, sufficiently lower than the frequency of the voltage loop that for this case is 224Hz. In Fig. 3, the flow diagram representing this algorithm is presented.

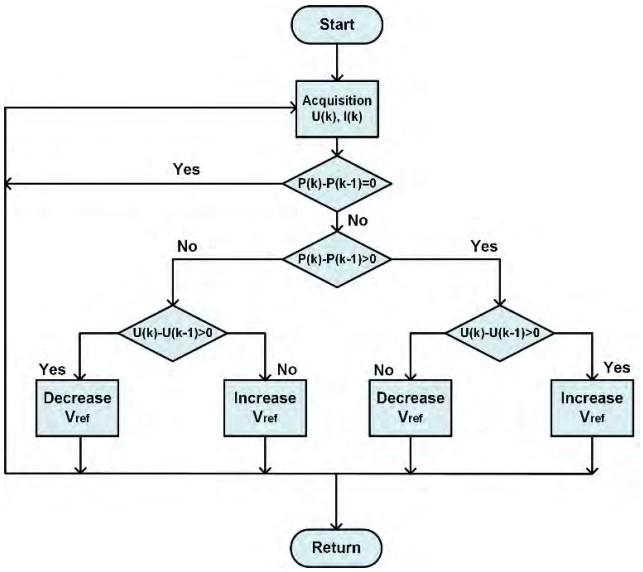

FIGURE 3. Flowchart of the P & O algorithm.

C. BOOST CONVERTER CONFIGURATION FOR GRID-CONNECTED OPERATION

Once the maximum power is obtained by means of the arrangement of solar panels, it is necessary to raise the voltage that is delivered to the inverter operating levels, in this case 400V *dc*. To achieve this goal a Boost converter is used and its development is presented below.

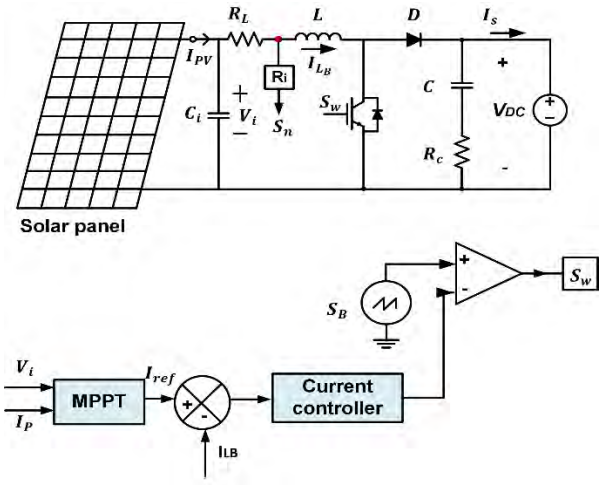

FIGURE 4. Block diagram of the Boost converter for grid-connected operation.

On the other hand, to increase the tension extracted from the arrangement panels, a Boots converter has been chosen; which is shown in Fig. 4 for this operation mode.

In the Fig. 4, the current control of the Boost converter is responsible for regulating the output of the MPPT algorithm; which is compared with the converter inductor current (L_B). The output of this controller is regulated by means of a PI controller, having as output the control voltage (v), which is used by the peak current mode-control circuit (CIC) [38]. This controller regulates the maximum current though the inductor of the Boost converter.

Finally, an external stabilization ramp (S_B) is compared with the output signal current controller, used to trigger control of the converter power switch. The modeling and design of the Boost converter is presented in detail in [39]. The waveforms of the Boost converter for the operation mode grid-connected are presented in Fig. 5. In this figure, the waveforms of the current can be seen in the presence of variations in irradiance in the photovoltaic panel; having a power change proportional to this variation. However, is have a constant *dc* voltage as the converter output, which results in an adequate performance of the Boost converter.

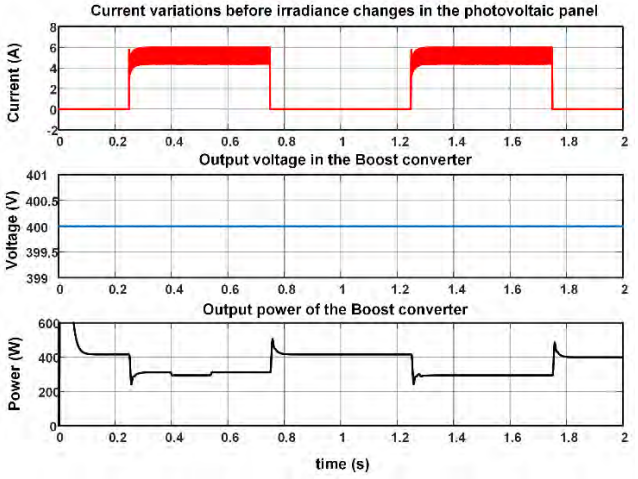

FIGURE 5. Boost converter waveforms for grid-mode operation.

Particularly, the inverter has two control loops, an internal loop called a current loop and an external loop called a voltage loop. This two-loop allows regulating the inverter output current and the DC_link voltage when the inverter is grid-connected and regulating the output current and voltage when it is connected in island mode. It should be noted that the current control is the same for both modes of operation and in addition to regulating the current its objective is to avoid high transients at the time of reconfiguration.

Particularly, for the current loop a resonant controller [40] is complemented to comply with IEEE 929-2000 [41] normative, for maximum total harmonic distortion of the current (THDi) injected to the grid. The resonant controller design is based on the theory of generalized integrators and is implemented at the grid frequency to comply with said standard. Likewise, an integral proportional control (PI) is designed for the voltage loop, which allows regulating the DC_link coltage.

TABLE 1. Inverter parameters.

Parameters	Value
Panel voltage variation (Vg)	70-96 V
Injected power by panel (P_{pv})	400 W
DC_LINK voltage (V_{DC})	400 V
Inverter output voltage (V_o)	230 V_{RMS}
Inverter output frequency (f_o)	50 Hz
Inverter output inductance (L)	9.57 mH
Inverter Output capacitor (C)	600 nF
Damping resistance (R_d)	5 Ω
Inverter switching frequency (f_{si})	20 kHz
Load resistance (R_{Load})	132 Ω
Boost inductance (L)	1.5 mH
Boost input resistance (R_L)	0.12 Ω
Boost output resistance	0.085 Ω
Boost output capacitor	1000 µF
Boost switching frequency (f_{sB})	20 kHz

TABLE 2. Summary of controller designed for grid mode operation.

Boost Converter			
Controller	Expression	Crossover frequency	Phase margin
PWM Modulator gain	$F_m = \frac{1}{S_e T_s} = \frac{1}{V_{pp}} = \frac{1}{20000 * 50\mu}$	2.2kHz	72.8°
Current controller	$G_{iRed}(s) = G_{ilsla}(s) = \frac{2500\ (s+80)}{s(s+62700)}$	1.7kHz	52°
Inverter			
Current controller	$K_P + \frac{K_h * B_h * s}{s^2 + B_h * s + (\omega_h^2)} = 1.32 + \frac{100 * (2\pi) * s}{s^2 + 2\pi * s + (100\pi)^2}$	2.0kHz	65.6°
DC_link Voltage controller	$-1 * \left(Kp + \frac{K_i}{s}\right) = -1 * \left(2. + \frac{0.09}{s}\right)$	15Hz	82°

In Table 1, the inverter parameter and Boost converter are shown.

In Table 2, the controllers design for the inverter and the Boost converter implemented for this mode of operation are reported.

Taking into account that the inverter can be reconfigured, that is to say, to pass from grid-connected operation to grid-disconnected operation, it is important to consider the use of island detection algorithms; with the purpose of increasing the reliability of the system reconfiguration. An algorithm based on the variation of active and reactive power is described below.

D. ISLANDING CONDITION

Islanding is the island condition in which a distributed generator (DG) continues to supply a direct local load even though

the power of the electric grid is no longer present. Island condition can be dangerous for distributed generation systems and for the same electricity grid, since at any given time, some circuit can be active and without taking it into account it can be reconnected automatically. In addition, if in island mode operation some strict frequency control is altered, this can cause large variations in frequency and voltage [42]. In an application as it is, where distributed generation is obtained by means of solar panels; at the moment that there is a power cut, the solar panel will continue to supply energy while the irradiance is sufficient. In this case, the circuit isolated by the interruption becomes an island. For this reason, solar inverter that are designed to supply power to the grid generally require some type of automatic anti-island circuit.

There are different islanding detection techniques that are divided into remote and local; the latter being divided into passive and active [43]. Considering this, in this work is chose to use an active method technique based on variation of active and reactive power. Which has the particularity of affecting in a controlled manner, voltage, frequency and other parameters associated with the inverter individually or in combination, when a change occurs that causes these variables to exceed a predetermined threshold. Therefore, through the positive feedback of the variable, if the grid is not connected, it is possible to reach the levels of over/under-voltage and over/sub-frequency, with which the islanding situation is detected; this technique is described below.

E. VARIATION OF ACTIVE AND REACTIVE POWER

This method is based on the injection of active and reactive power by the inverter to the grid. In islanding condition the power flows from the inverter to the local load, affecting the current and voltage at the Point Common Coupling (PCC), with this consideration, the variation of the voltage is directly proportional to the variation of active power. Therefore, it is possible to vary the active power injected by the inverter in order to bring the amplitude of the voltage out of the normal operating range and to detect the islanding.

Fig. 6 shows the block diagram of this technique. This method aims to vary the value of the voltage in the PCC until it can be detected as an over/under voltage (Vos). Depending on the value of the Kv gain, there will be a shorter or longer response time, however, it must be taken into account that a very high value could generate instability if any disturbance occurs, factor that increases or decreases the term *dP* proportional to the variation of the voltage.

An initial value of the constant can be obtained in the following way, $Kv = 2\sqrt{(P_{DG}/R_L)}$; where: P_{DG} is the distributed generator power and R_L is the load equivalent resistance. The current reference in the inverter control can be calculated with the expression (1).

$$I_{ref} = \frac{dP + P_{DG}}{V_{0s}} \tag{1}$$

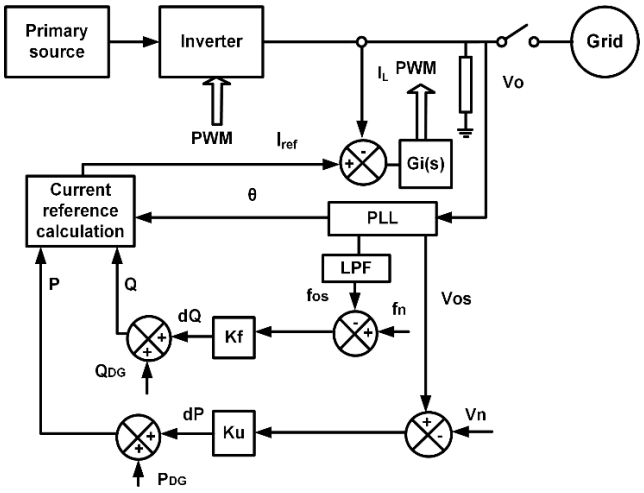

FIGURE 6. Block diagram of the injection method of P and Q.

where, $P_{DG} = P_L = {V_o^2}/{R_L}$ and $dP = Kv\,(V_{OS}\text{-}V_n)$, also V_{OS} is the measurement of the amplitude of the inverter output voltage.

The inverter reconfiguration of the grid-connected operation to grid-disconnected operation, is presented with the change of the voltage controller, since the controller used in grid mode has to regulate the DC_link voltage; while for the grid-disconnected operation, its output voltage is controlled. Additionally, the reference for the voltage controller in grid-disconnected operation is fixed by the droop schemes, while for the grid mode it is constant. In order to avoid abrupt transitions from one operation mode to another, the final conditions of the controllers in one operation mode are matched to the initial conditions of the controller in the other operation mode. It should be noted that when switching from one operation mode to another, the same inverter output current controller is used. That is, initially, the inverter output current control is designed for grid-connected operation, and it is used in the reconfiguration to grid-disconnected operation, which allows to limit the current and provides protection to the system [44].

The development of the inverter for its grid-disconnected operation is described below.

III. INVERTER CONFIGURATION FOR GRID DISCONNECTED OPERATION

The inverter configuration for grid-disconnected operation is presented in Fig. 7, in this inverter operating mode behaves as a voltage source and this must feed a local load. With this consideration, the inverter must maintain the waveform, amplitude and the frequency of the output voltage signal that must be delivered to the load; as in this operation mode the inverter controls its output voltage, it is obvious that it cannot regulate its *dc* voltage from its input. With this criterion, the Boost converter must simultaneously regulate both its input current and the output voltage that would correspond

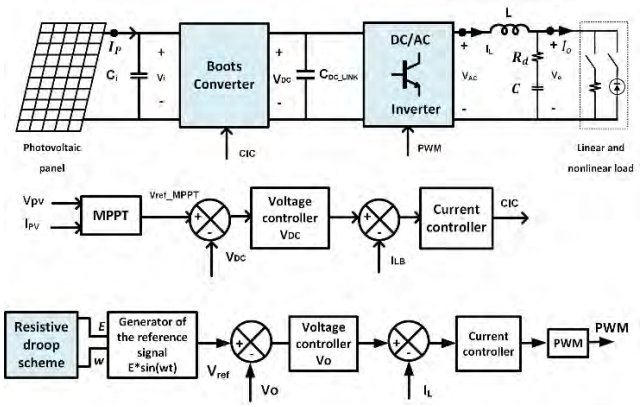

FIGURE 7. Block diagram of the inverter for grid- disconnected operation.

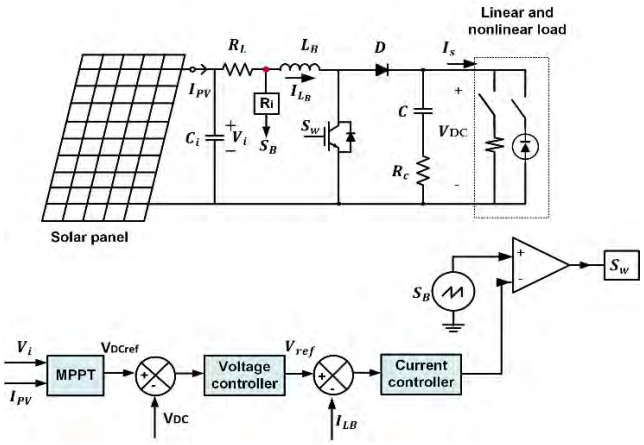

FIGURE 8. Block diagram of the Boost converter for the grid-disconnected operation.

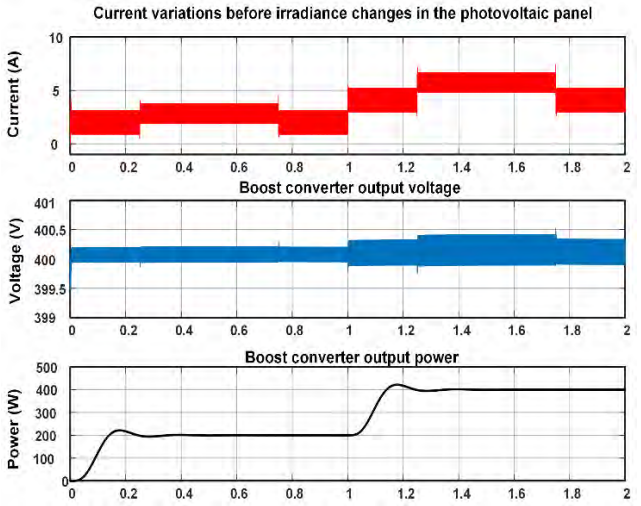

FIGURE 9. Boost converter waveforms for grid disconnected operation.

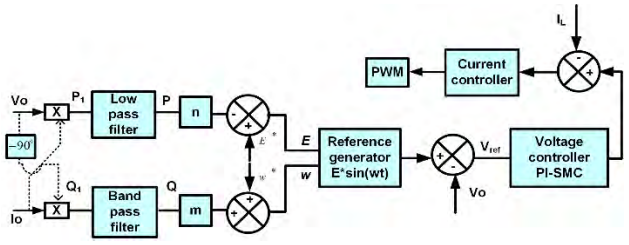

FIGURE 10. Droop Scheme with resistive character.

to the inverter input voltage (V_{DC}) which solves the problem. The input current is adjusted by closing the current control loop, called the internal loop, while the output voltage is regulated by means of and additional control loop, called the external loop, as shown in Fig. 8.

The waveforms of the Boost converter for the island mode operation are presented in Fig. 9. In this figure, you can see the waveforms of the current before variations in irradiance in the photovoltaic panel, and proportional changes in power before this variation. However, at the converter output, a *dc* voltage with a small ripple is present, which results in an adequate performance of the Boost converter.

On the other hand, in grid-disconnected operation it is important to consider the parallel connection of different inverters, for which a droop schema is implemented that fulfill this purpose.

A. DROOP SCHEMES

In grid-disconnected operation, the total power delivered by this is the one demanded by the local load; therefore, the active power and the reactive power consumed by it must be taken into account.

This consideration allows the reference voltage to be obtained for the inverter, giving rise to an adequate performance of this. To achieve this, a droop scheme is implemented [45].

Droop schemes have traditionally been applied to synchronous generator control connected in parallel in power systems. However, it has recently been used in the control of Distributed Generators (DGs) with the same goal to share power according to demand [46].

In particular, for this application it was decided to use a droop scheme with a resistive characteristic, considering that the output impedance closed loop inverter presented a resistive behavior when implementing the controllers for this operation mode, which resulted in a good performance converter. Fig. 10, shows a droop scheme with resistive characteristics and is used to give the voltage reference to the voltage controller in this case an integral sliding mode controller.

The active and reactive power that an inverter can provide to the load in a general way can be expressed in (2) and (3).

$$P = \frac{E \cdot V}{Z} \cdot \cos\emptyset - \frac{V^2}{Z} \tag{2}$$

$$Q = -\frac{E \cdot V}{Z} \cdot \sin\emptyset \tag{3}$$

where Z is the inverter output impedance, Φ is the phase angle between the inverter output voltage and the common bus voltage; E and V are the amplitude of the inverter output voltage and the load voltage respectively.

Assuming that the inverter output impedance is resistive, in the expressions (2) and (3) ($Z = R$ y $\Phi = 0°$) and the power angle is very small, then the active and reactive power are written as in the expressions (4) and (5).

$$P = \frac{E \cdot V}{R} \cdot \cos\emptyset - \frac{V^2}{R} \approx \frac{V}{R} \cdot (E - V) \tag{4}$$

$$Q = -\frac{E \cdot V}{R} \cdot \sin\emptyset \approx -\frac{E \cdot V}{R} \cdot \emptyset \tag{5}$$

Consequently, the active power can be regulated by voltage amplitude of the inverter output, while the reactive power can be controlled by the inverter frequency. With these considerations, when the inverter output impedance is highly resistive, the droop scheme for P and Q is represented by means of expressions (6) and (7), where it is established that by means of the amplitude E and the frequency ω of the inverter output voltage, the active and reactive power flow can be regulated respectively.

$$\omega = \omega^* + m * Q \tag{6}$$

$$E = E^* - n * P \tag{7}$$

Being, ω^* and E^* the angular frequency and output voltage amplitude without load, and m and n are the droop coefficients for frequency and amplitude respectively. It is relevant to mention that a high value of the coefficients of the droop allows an adequate power distribution; however, as consequence there is a bad voltage regulation. Therefore, the choice of an appropriate value of these coefficients will allow the inverters to exhibit adequate transient response behavior, stability and accuracy in power distribution [47].

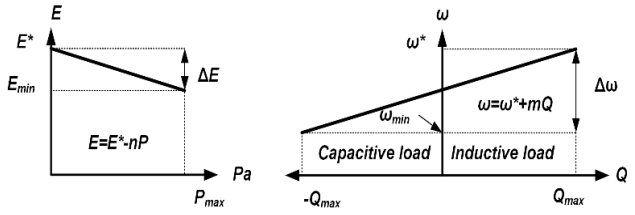

FIGURE 11. Voltage and frequency characteristics of the resistive droop scheme.

Fig. 11 shows the voltage and frequency characteristics of the droop scheme with resistive characteristic. The coefficients values m and n are chosen to guarantee the system stability [48]; they are determined by the expressions (8) and (9).

$$m = \frac{\Delta_\omega}{Q_{max}} \tag{8}$$

$$n = \frac{\Delta_E}{P_{max}} \tag{9}$$

where P_{max} and Q_{max} are the maximum active and reactive power that can be delivered by the inverter. In addition, $\Delta\omega$ and Δ_E are the maximum allowed deviations of frequency and amplitude of the inverters output voltage. These values are determined taking into account that it must maintain an adequate distribution of active and reactive power between energy conversion units, guaranteeing its stability. For application, the values of m and n are 0.001.

Having the value of P_{max}, the active power P can be obtained by implementing a low pass filter (LPF); in addition, it must be considered that the output voltage must be offset 90°, therefore it is necessary to use a low pass filter. The value of Q is obtained in a similar way; however, in order to be able to synchronize different inverter with a good performance considering possible frequency variation and therefore phase deviations, it is required to eliminate the *dc* component of the reactive power. To meet this objective, a low-pass filter connected in cascade with a high-pass filter is implemented; resulting in a bandpass filter (BPF).

The expressions of the low pass filters for P and Q are presented in equations (10) and (11), respectively:

$$Q_{LPF} = \frac{1}{31.83 \cdot 10^{-3} \cdot s + 1} \tag{10}$$

$$P_{LPF} = \frac{1}{31.83 \cdot 10^{-3} \cdot s + 1} \tag{11}$$

$$H_{BPF}(s) = \tau^{-1}\omega_c \cdot \frac{s}{(s+\tau^{-1}) \cdot (s+\omega_c)} \tag{12}$$

where ω_c is the cut-off frequency of the band-pass filter, which is chosen below a decade of the grid frequency.

Finally, the low pass filter block of Fig.10 must be redesigned for a band pass filter, which is presented in (13).

$$H_{BPF}(s) = \frac{s}{0.3183 \cdot s + 1} \cdot \frac{1}{31.83 \cdot 10^{-3} \cdot s + 1} \tag{13}$$

Finally, in grid-disconnected operation, it is convenient to implement controllers that improve the disturbances rejection, which occur when the inverter feeds non-linear load. To fulfill this objective, an integral sliding mode control is designed, which is described below.

B. INTEGRAL SLIDING MODE CONTROLLER (ISMC)

For grid-disconnected operation, the use of a sliding mode controller is proposed, which aims to reduce the total harmonic distortion that occurs when in this inverter operating mode feed non-linear load. In addition, in the reconfiguration of grid mode to island mode avoids excessive transients, which is achieved considering that this controller presents a rapid dynamic response.

Fig. 12 shows the block diagram of an integral sliding mode controller (ISMC) that is implemented in the voltage loop of the inverter [49]. In this block diagram, it can be seen that the voltage controller receives a reference signal from a droop scheme.

The convergence parameter of the proposed ISMC controller is achieved through the design of a *PI* controller, which must meet the Nyquist stability criteria; the design parameters of this regulator are those shown in Table 3. This PI controller ensures that the control of sliding modes reaches the reference to follow and remains in it; ensuring that it reaches the gliding surface more quickly and stays there. This is achieved considering that the error and its derivative will have opposite

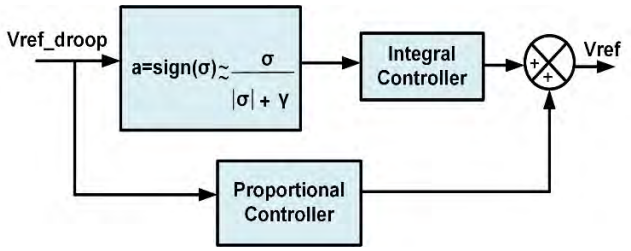

FIGURE 12. Integral sliding mode control scheme.

TABLE 3. Summary of controller designed for grid-disconnected operation.

Boost Converter			
Controller	Expression	Crossover frequency	Phase margin
Voltage controller	$G_{vIsland}(s) = \frac{0.18\,(s+617)}{s}$	199Hz	62.2°
Current controller	$G_{Island}(s) = \frac{2500(s+80)}{s(s+62700)}$	1.7kHz	52°
Inverter			
Current controller	$K_P + \frac{K_h * B_h * s}{s^2 + B_h * s + (\omega_h^2)} = 1.32 + \frac{100 * (2\pi) * s}{s^2 + 2\pi * s + (100\pi)^2}$	2.0kHz	65.6°
Voltage Controller ISMC	$Kp + K_i * u = 0.8 + 3000 * \frac{\sigma}{\lvert\sigma\rvert + 0.5}$	978Hz	68.4°

signs during its operation fulfilling the condition of existence, that is, $\lim_{s\to 0} s\dot{s} < 0$.

The integral sliding mode controller is designed from the following procedure: initially the PI controller is implemented in the external control loop and the SMC control is implemented in cascade with the integral action using the "sigmoid function" approximation given by (14).

$$u = sign(\sigma) \approx \frac{s}{|s| + \gamma} \tag{14}$$

where σ is the sliding variable, and the function sign (σ) is equal to 1 when $\sigma \geq 0$, and equal to -1 when $\sigma < 0$. In addition, γ is a pre-feeding term whose value is adjustable; particularly for this application, it has a value of 0.5.

For the correct integral sliding mode control design, it is recommended initially to design an integral proportional controller (PI) to ensure the stability of the system; to which additional control of sliding modes. This combination is configured by means of a proportional control plus an integral control, where the latter will be in cascade with the sliding modes control. The expression (15) shows this structure.

$$P{+}I{*}SMC = K_p + K_i \cdot u \tag{15}$$

Table 3, reports the designs and values of the controllers obtained for inverter in grid-disconnected operation (island mode). Details on the adjustment of some of the controllers in island mode can be found in [39], [50]. Particularly, the integral sliding mode control design for this operation mode, it was reported in the previous section.

The Implementation complexity of the control system proposed for this application is simple, considering that its design is based on a cascade control configuration; presenting controllers in internal and external control loops with a hierarchy established by this configuration; both for the regulation of the *dc-dc* converter and for the inverter. For the configuration in grid-connected mode, the Boost converter regulates the panel current maintaining a constant output voltage of 400V, which will be the inverter input voltage (Voltage in the DC_Link). In this operation mode it is important to synchronize the inverter frequency with the grid frequency for its connection, which is achieved through the PLL. Once the inverter is synchronized, it will regulate the voltage in the DC_Link and the current that is injected into the grid. For the grid-disconnected operation, the Bosst converter is responsible for regulating its output voltage and panel current. In addition, the inverter is responsible for regulating the current and voltage that must be supplied to the local load. In this operation mode an integral sliding mode controller is implemented in order that the inverter presents a better disturbance rejection.

Finally, the droop schemes are implemented with the purpose of giving the reference to follow by voltage control for island mode operation; in addition to allowing the parallel connection of different inverters achieving with this the distribution of active and reactive power between them.

In the next section, the results of the inverter's performance are shown during its reconfiguration, that is, in the transition between both modes of operation. That is, from the grid-connected operation to the grid-disconnected operation. It is important to mention that the simulations were carried out taking into account that in grid-disconnected operation, the inverter feeds linear and non-linear loads.

IV. SIMULATION RESULTS

The inverter parameters to evaluate its performance by means of simulation in the PSIM^{TM} software [51] are reported in Table 1. It should be noted that the simulations presented consider the interconnection of two parallel connected inverters and grid-interconnected. These simulations are presented, feeding linear and non-linear load.

A. INVERTER RECONFIGURATION FROM GRID-CONNECTED MODE TO GRID-DISCONNECTED MODE

In the inverter reconfiguration from the grid-connected mode to grid-disconnected mode, the controllers must also be reconfigured, considering that in this new operation mode the inverter has to feed a local load. That is, in grid mode the inverter regulates the voltage in the DC_link and the

current that is injected into the grid, while in this new mode of operation (island), what must be regulated is the inverter output current and voltage that must be supplied to the local load. An important aspect to consider in this operation mode is that the voltage reference is provided by the resistive droop scheme.

Likewise, the Boost converter changes its configuration in order to regulate its output voltage (V_{DC}) and its input current (I_{LB}). Likewise, the Boost converter changes its configuration in order to regulate the voltage in the DC_link and its input current. An important aspect that should be highlighted is that to avoid severe transitions in the reconfiguration, the current connected mode [52] controller that is designed for the grid-connected mode is the same one used for reconfiguration to island [53].

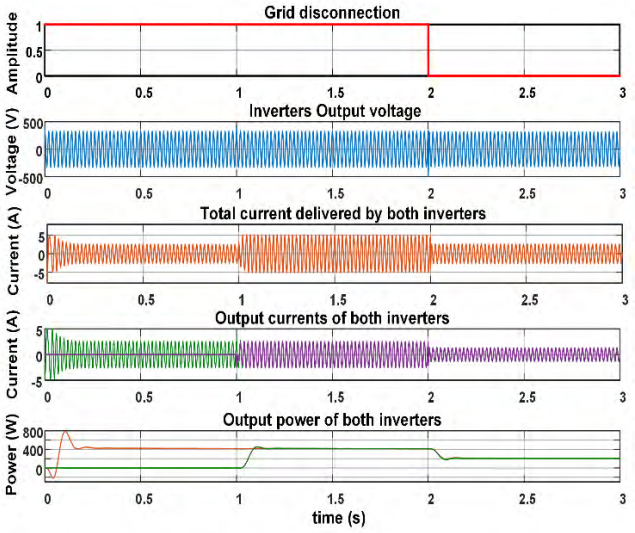

FIGURE 13. Inverter reconfiguration of grid-interconnected mode to grid-disconnected mode with linear load.

B. INVERTER RECONFIGURATION WHEN IT FEED LINEAR LOAD

Fig. 13 shows the waveforms of the two inverters, particularly when the first is connected to the grid and the second is connected in parallel with the first; as well as the transition from grid-connected to grid-disconnected mode. It is important to note that for island mode operation the integral sliding mode control was implemented, whose design was previously reported.

To observe the performance of the designed controllers for the different inverter control loops, the simulation was performed at the moment of the interconnection between two inverters when they are in grid-connected. In this simulation it can also be observed how at the moment of disconnection of both inverters with the grid; these are distributed to the nominal load, observing a good performance of both inverters. Also, the transients in the inverter connection and in the transition from grid-connected mode to disconnected mode are of low magnitude. Particularly in the inverters disconnection, the integral sliding mode controller presents a good performance, considering that it presents a very fast dynamic response.

Fig. 14 shows the waveforms at the precise moment when the inverter is disconnected from the grid and it is fed a load of 132.94 Ω.

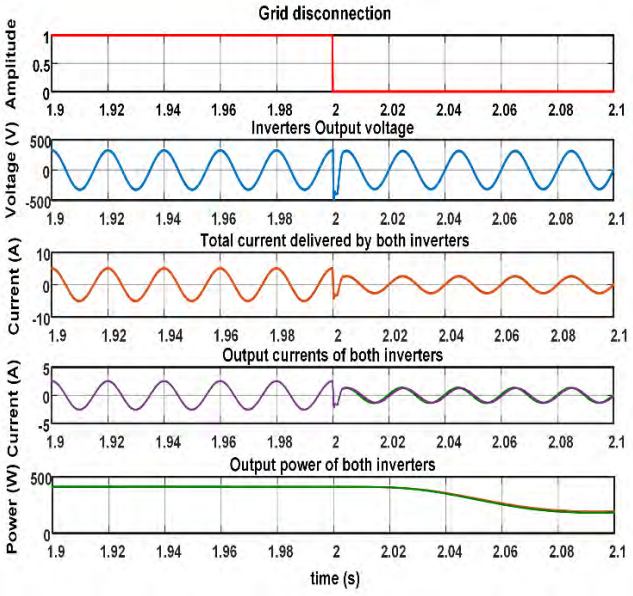

FIGURE 14. Reporting of inverter signals at the time of transition with linear load.

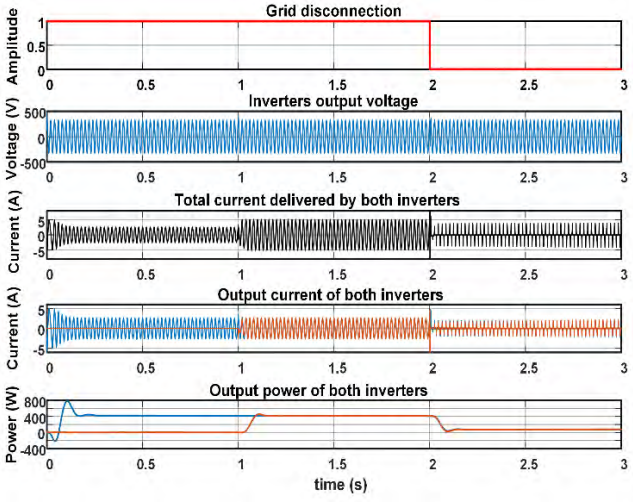

FIGURE 15. Inverter reconfiguration of grid-interconnected mode to grid-disconnected mode with non-linear load.

C. INVERTER RECONFIGURATION WHEN IT FEED NON-LINEAR LOAD

Fig. 15 shows the waveforms of the two inverters, when they are fed non-linear load.

As in the previous case, to observe the performance of the controller designed for the different inverter control loops,

the simulation was performed at the instant of the parallel connection of two inverters in grid-connected operation. In addition, we observe the instant in which the disconnection of both inverters occurs, going from grid connected operation to island mode. In this simulation, a good controller performance is observed, considering that the transients in the interconnection of the two inverters and in the transition from the grid mode to the island mode is of low magnitude.

As can be seen in Fig. 15, particularly for operation in island mode, the integral sliding mode control implemented showed excellent performance both at the time of disconnection and when operating non-linear load.

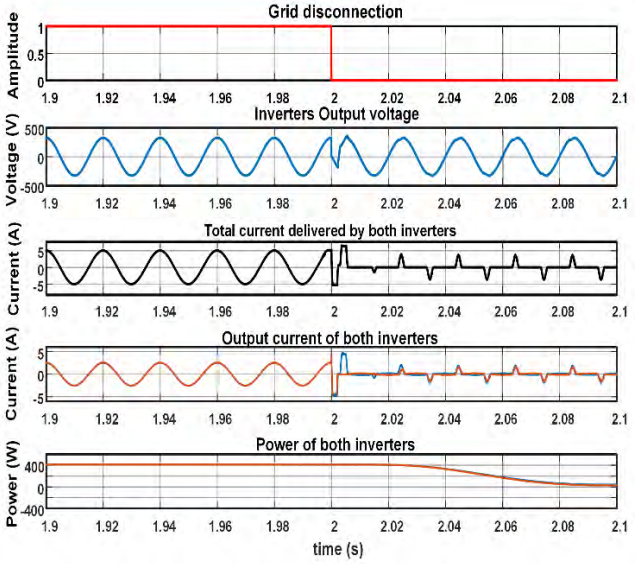

FIGURE 16. Reporting of inverter signals at the time in which the inverters is grid-disconnect and feeding non-linear load.

Fig. 16 shows the waveforms in the instant when the inverter is grid-disconnect and switch to island mode operation, feeding non-linear load with the following features.

A full-wave rectifier bridge, a resistor in parallel with a capacitor that is connect to the rectifier output with values of 680 Ω and 96μF respectively; resulting in the load having a crest factor (CF=4.2). The configuration of the load is presented in Fig. 17.

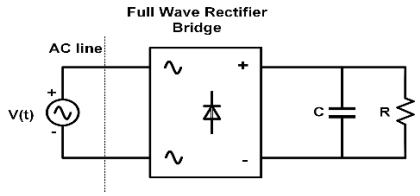

FIGURE 17. Configuration of non-linear load.

D. INVERTER RECONFIGURATION FROM GRID-DISCONNECTED MODE TO GRID-CONNECTED MODE

If the inverter is working in grid-disconnected operation, it is possible to reconnect it to the grid; this is done by synchronizing the phase of the inverter output voltage with the phase of the grid voltage. This action is achieved by measuring the corresponding phases and allowing their difference to be reduced to zero through a synchronization loop. To achieve this objective two PLLs are used to measure the grid phase and the inverter phase respectively, in such a way that when both are equal their connection is possible [50]. Considering criteria of controllers design, in the same way as in the grid-connected operation transition to operation disconnected from it; in order to avoid abrupt transitions from one mode to another it is necessary to equalize the final conditions of the controllers in one operation mode to the initial conditions of the controller in the other. Also, the inverter output current controller designed for grid connected operation is used, which allows to limit the current in the transition and provides protection to the system.

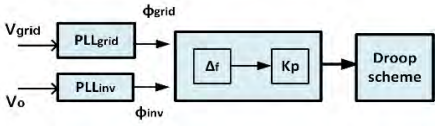

FIGURE 18. Block diagram of synchronization.

The synchronization block diagram is presented in Fig. 18, where: Δf is the phase difference between the inverter and the grid and Kp is the frequency proportional constant, the phase is expressed in radians. For this application, a value of Kp = 0.17 allows a correct synchronization between the grid and inverter.

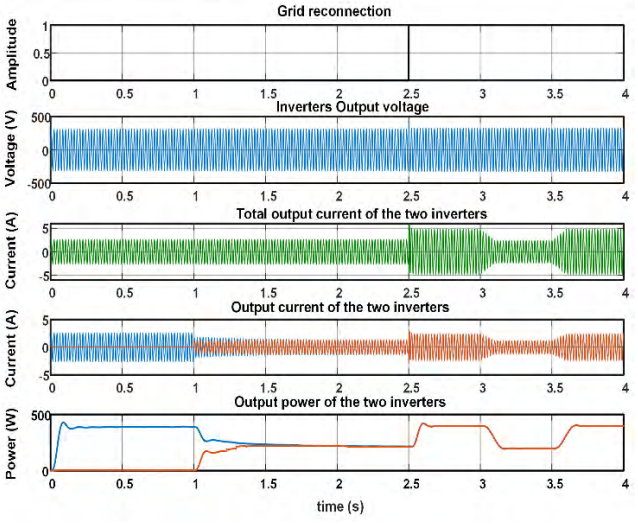

FIGURE 19. Inverter reconfiguration of grid-disconnected mode to grid-reconnected mode with linear load.

E. INVERTER RECONFIGURATION WHEN IT FEED LINEAR LOAD

In Fig. 19, the waveforms of the two inverters are shown, particularly when the number one, operates in island mode

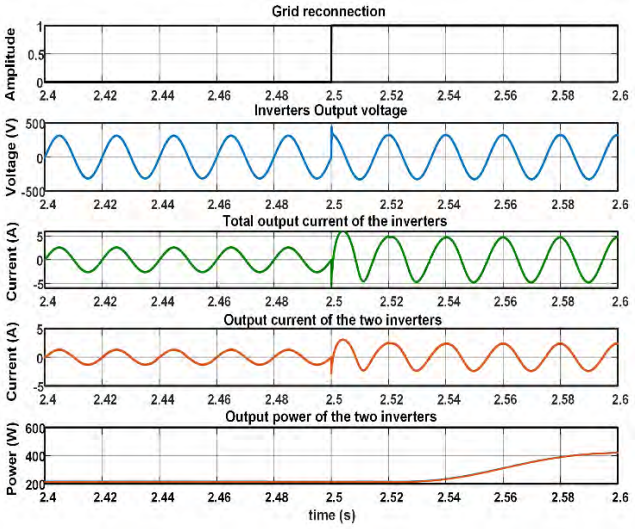

FIGURE 20. Reporting of inverter signals at the time when the inverters are reconnected to the grid.

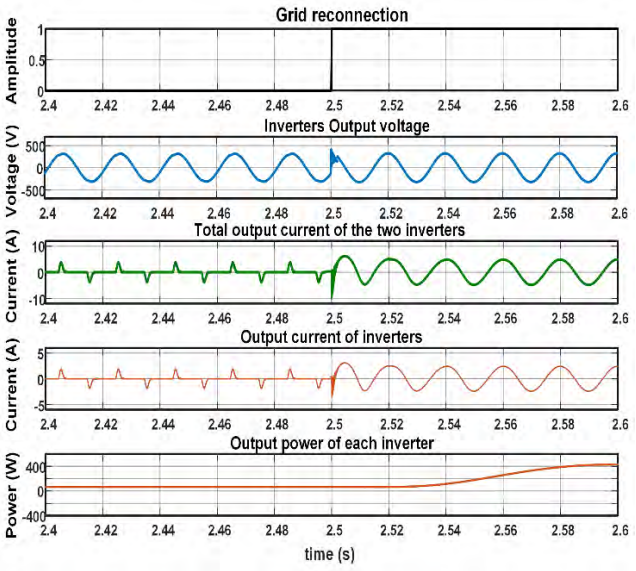

FIGURE 22. Reporting of inverter signals at the time in which the inverters is grid-reconnected and feeding non-linear load.

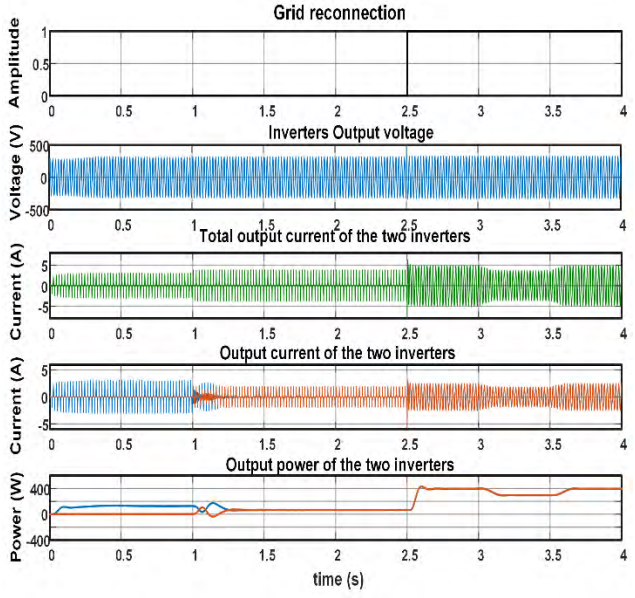

FIGURE 21. Inverter reconfiguration of grid-disconnected mode to grid-reconnected mode with non-linear load.

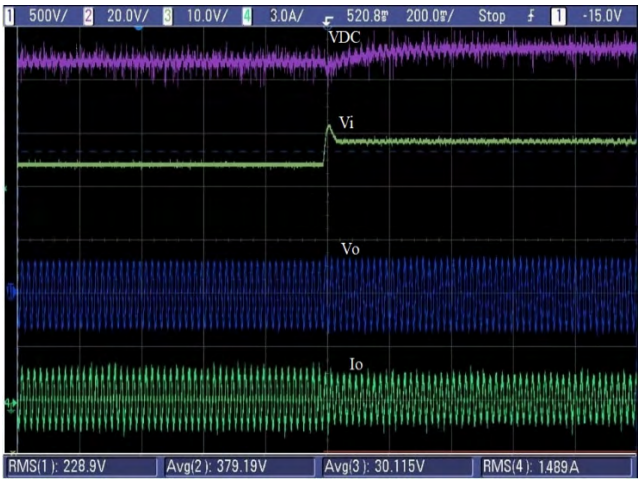

FIGURE 23. Transient response of the transition from grid-connected operation to grid-disconnected operation. V_{DC} (firt graph, 20 V/div), V_i (second graph, 10 V/div), v_O (third graph, 500 V/div), *io* (fourth graph, 3A/div).

and the number of two is connected in parallel with number one; as well as the transition from operation in island mode to grid-connected mode. It is important to remember that for operation in island mode the integral sliding mode control was implemented, whose design was previously reported.

In this simulation it is also observed how, at the instant of reconnection, each inverter injects its nominal current into the grid; a good inverter performance is observed, since the transients during the parallel connection of the two inverter and in the reconfiguration from grid-disconnected operation a grid-connected operation are of low magnitude. Fig. 20, shows the waveforms at the instant in which the inverters are reconnected to the grid by injecting each of these its nominal current.

A good performance of the inverters is observed, since the transients in the parallel connection of inverters and in the change from disconnected mode a grid-connected operation are of low magnitude. As shown in Fig. 21, particularly for island mode operation, the integral sliding mode control has a good performance both for the parallel connection of the two inverters feeding non-linear load, and in the interconnection with the grid. Fig. 22, shows the waveforms at the instant in which the inverters are grid-reconnected by injecting each of these its nominal current.

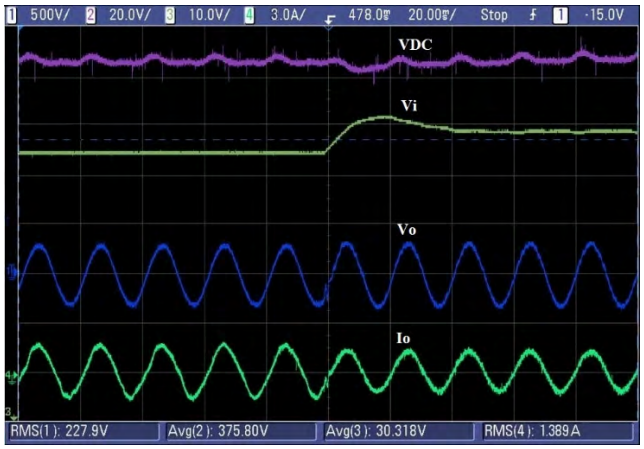

FIGURE 24. Detail the waveforms of transient response of the transition from grid-connected operation to grid-disconnected operation n. V_{DC} (firt graph, 20 V/div), V_i (second graph, 10 V/div). v_O (third graph, 500 V/div). *io* (fourth graph, 3A/div).

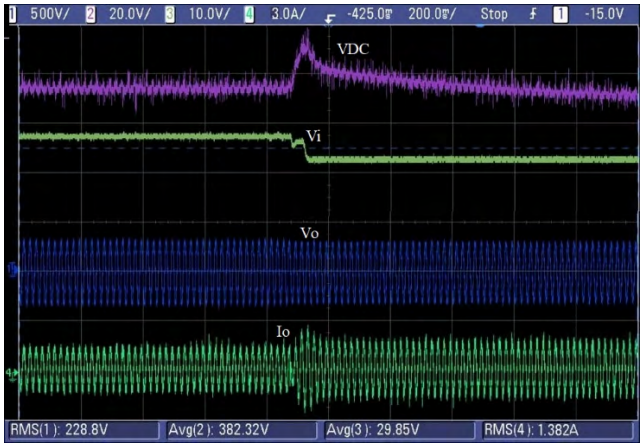

FIGURE 25. Transient response of the transition from grid-disconnected operation to grid-connected operation. V_{DC} (firt graph, 20 V/div), V_i (second graph, 10 V/div), v_O (third graph, 500 V/div), *io* (fourth graph, 3A/div).

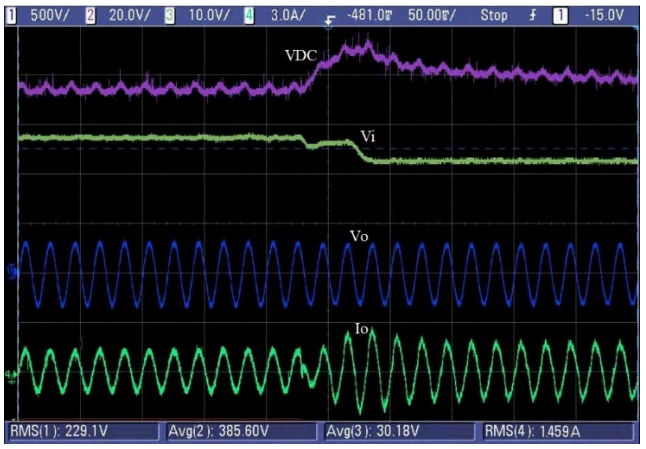

FIGURE 26. Detail the waveforms of transient response of the transition from grid-disconnected operation to grid-connected operation. V_{DC} (firt graph, 20 V/div), V_i (second graph, 10 V/div), v_O (third graph, 500 V/div), *io* (fourth graph, 3A/div).

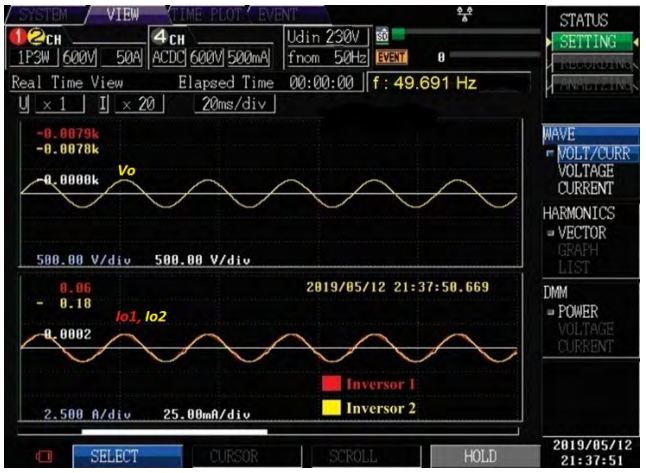

FIGURE 27. Waveforms of Output voltage v_O (first graph, 500 V/div), and output current of two inverters connected in parallel in grid-disconnected operation *io* (second graph, 3A/div).

V. EXPERIMENTAL RESULTS

Experimental tests were carried out to validate the performance controllers implemented in the 400 W photovoltaic inverter; which are reported in Tables 2 and 3 respectively. These controllers is implemented in a TMDSC-NCD28335 digital signal processor (DSP), at a sampling frequency of 40 kHz. A programmable power supply AMREL SPS800-12-D-013 is used to perform these tests.

Fig. 23 shows the transition from grid-connected operation to grid-disconnected operation (island detection) with a local load of 170 Ω (330 W at 230 Vrms). As it can be observed, the inverter can, with a smooth transient, switch from grid-connected operation to grid-disconnected operation while regulating the output voltage quickly to the nominal operating range. In grid-connected operation, the inverter output current follows a reference that allows to inject the maximum available power from the programmable *dc* source, whereas in grid-disconnected operation, the output current follows the reference imposed by the droop schemes (load). In this case, the resistive load absorbs a smaller power (330 W) than that injected to the grid before islanding (400 W). Additionally, the inverter input voltage is adjusted by a P&O and MPPT algorithm to follow the load power consumption.

Fig. 24 shows in detail the waveforms of Fig. 23, particularly, at the instant in which the transition from grid-connected operation to grid-disconnected operation of the converter occurs. In Fig. 23 you can observe that the steady-state value of V_{DC} in island mode is slightly higher (380 V) than in grid-connected mode (370 V) approximately.

Fig. 25 shows the transition from grid-disconnected operation to grid-connected operation. In this test the objective is that once the grid voltage and the inverter are synchronized, the grid switch returns to its closed state; this transition does not present a significant transient. In this test, the inverter feeds a load of 330 W in grid-disconnected operation. Also, after the transition, the inverter injects the energy supplied by the programmable source *dc* to the grid, in this case 400 W.

Fig. 26 shows a detail of Fig. 25, in which a good transient response of the transition from grid-disconnected operation to grid-connected operation, is observed.

Fig. 27, PW3198 the HIOKI network analyzer was used to show the voltage and current waveforms of two parallel connected inverters, feeding a resistive load of 170 ohms. In this graph it is observed that the two inverters is distribute the total load by supplying similar currents and keeping the voltage constant.

VI. CONCLUSIONS

This paper reports the inverter operation in two operation modes: grid-connected mode and disconnected mode, as well as its reconfiguration for both operation modes; that is, its transition from grid-connected mode to disconnected mode as well from grid-disconnected mode to connected mode. In particular, in grid-connected operation, the inverter regulates its input voltage (output voltage the Boost converter) and output current (current injected into the grid). In addition, in grid-disconnected operation, the inverter regulates its output voltage (voltage at the local load) and output current (current at the local load). In both operating situations, the Boost converter receives the voltage from a solar panel. For inverter grid-disconnected operation, a droop scheme is implemented that allows obtaining the reference voltage from the measurement of the active and reactive power demanded by the local load, as well as allowing the parallel connection of inverters in order to meet increases in load consumption. Considering this, the main this work contribution is the implementation of an integrals sliding mode controller for grid-disconnected operation that meets two important objectives. First, it allows the transition from grid-interconnected mode to disconnected mode to be performed with good performance; and the second, allows that in grid-disconnected operation, its reducing the THDv to values below 5%, which is recommended according to the regulations IEEE Std. 929, 2000 being of a value of 2.2%. Another important aspect that is reported in this work is that for inverter grid-disconnected operation, simulations are developed feeding linear load, highlighting the simulations feeding non-linear load, considering that in practical situations it is not linear in general. In addition, the development of energy conversion topologies based on two power systems is presented: *dc-dc* converter and inverter. Finally, the inverter's performance during its reconfiguration from one operation mode to another is validated by means of simulations and experimental tests.

As future work, it is proposed to design and develop the controller for hierarchical levels of three and four in order that the microgrid operates intelligently managing the power generation resources in an optimal way. Also, it is proposed to develop as a complement to this work the storage of energy in batteries, obtained from the arrangement of solar panels.

REFERENCES

[1] H. Farhangi, "The path of the Smart grid," *IEEE Power Energy Mag.*, vol. 8, no. 1, pp. 18–28, Jan./Feb. 2010.

[2] J. Momoh, *Smart Grid: Fundamentals of Design and Analysis*. Hoboken, NJ, USA: Wiley, 2012.

[3] R. H. Lasseter, "Smart distribution: Coupled microgrids," *Proc. IEEE*, vol. 99, no. 6, pp. 1074–1082, Jun. 2011.

[4] M. Noussan, "Performance based approach for electricity generation in smart grids," *Appl. Energy*, vol. 220, pp. 231–241, Jun. 2018. doi: 10.1016/j.apenergy.2018.03.092.

[5] P. Järventausta, S. Repo, A. Rautiainen, and J. Partanen, "Smart grid power system control in distributed generation environment," *Annu. Rev. Control*, vol. 34, no. 2, pp. 277–286, 2010.

[6] J. A. P. Lopes, C. L. Moreira, and A. G. Madureira, "Defining control strategies for microgrids islanded operation," *IEEE Trans. Power Syst.*, vol. 21, no. 2, pp. 916–924, May 2006.

[7] J. C. Vásquez, J. M. Guerrero, J. Miret, M. Castilla, and L. G. De vicuña, "Hierarchical control of intelligent microgrids," *IEEE Ind. Electron. Mag.*, vol. 4, no. 4, pp. 23–29, Jan. 2010.

[8] C. Wang, J. Yan, C. Marnay, N. Djilali, E. Dahlquist, J. Wu, and H. Jia, "Distributed energy and microgrids (DEM)," *Appl. Energy*, Vol. 210, pp. 685–689, Jan. 2018

[9] S. Parhizi, H. Lotfi, A. Khodaei, and S. Bahramirad, "State of the art in research on microgrids: A review," *IEEE Access*, vol. 3, pp. 890–925, 2015.

[10] N. Abbassi and S. Reichert, "Novel control structure for grid connected and islanding inverters," in *Proc. 7th IET Int. Conf. Power Electron., Mach. Drives (PEMD)*, Manchester, U.K., 2014, pp. 1–5.

[11] J. Zhang, Q. Wang, C. Hu, and T. Rui, "A new control strategy of seamless transfer between grid-connected and islanding operation for microgrid," in *Proc. 12th IEEE Conf. Ind. Electron. Appl. (ICIEA)*, Siem Reap, Cambodia, Jun. 2017, pp. 1729–1732.

[12] S.-H Hu, C.-Y. Kuo, T.-L. Lee, and J. M. Guerrero, "Droop-controlled inverters with seamless transition between islanding and grid-connected operations," in *Proc. IEEE Energy Convers. Congr. Expo.*, Phoenix, AZ, USA, Sep. 2011, pp. 2196–2201.

[13] Z. Zeng and W. Shao, "Reconnection of micro-grid from islanded mode to grid-connected mode used sliding Goertzel transform based filter," *IET Renew. Power Gener.*, vol. 11, no. 7, pp. 1041–1048, 2017.

[14] X. Hou, Y. Sun, J. Lu, X. Zhang, L. H. Koh, M. Su, and J. M. Guerrero, "Distributed hierarchical control of AC microgrid operating in grid-connected, islanded and their transition modes," *IEEE Access*, vol. 6, pp. 77388–77401, 2018.

[15] O. Palizban and K. Kauhaniemi, "Hierarchical control structure in microgrids with distributed generation: Island and grid-connected mode," *Renew. Sustain. Energy Rev.*, vol. 44, pp. 797–813, Apr. 2015.

[16] T. L. Vandoorn, J. D. M. De Kooning, B. Meersman, and Y. L. Vandevelde, "Review of primary control strategies for islanded microgrids with power-electronic interfaces," *Renew. Sustain. Energy Rev.*, vol. 19, pp. 613–628, Mar. 2013.

[17] A. Bidram and A. Davoudi, "Hierarchical structure of microgrids control system," *IEEE Trans. Smart Grid*, vol. 3, no. 4, pp. 1963–1976, Dec. 2012.

[18] Q.-C. Zhong and Y. Zeng, "Universal droop control of inverters with different types of output impedance," *IEEE Access*, vol. 4, pp. 702–712, 2016.

[19] D. E. Olivares, A. Mehrizi-Sani, A. H. Etemadi, C. A. Cañizares, R. Iravani, M. Kazerani, A. H. Hajimiragha, O. Gomis-Bellmunt, M. Saeedifard, R. Palma-Behnke, G. A. Jiménez-Estévez, and N. D. Hatziargyriou, "Trends in microgrid control," *IEEE Trans, Smart Grid*, vol. 5, no. 4, pp. 1905–1919, Jul. 2007.

[20] J. M. Guerrero, J. C. Vasquez, J. Matas, L. G. de Vicuna, and M. Castilla, "Hierarchical control of droop-controlled AC and DC microgrids—A general approach toward standardization," *IEEE Trans. Ind. Electron*, vol. 58, no. 1, pp. 158–172, Aug. 2011.

[21] A. J. Wood and B. F. Wollenberg, *Power Generation, Operation, and Control*. Hoboken, NJ, USA: Wiley, 2013.

[22] E. Mojica-Nava, C. A. Macana, and Y. Quijano, "Dynamic population games for optimal dispatch on hierarchical microgrid control," *IEEE Trans. Syst., Man, Cybern. Syst.*, vol. 44, no. 3, pp. 306–317, Mar. 2014.

[23] S.-J. Ahn and S.-I. Moon, "Economic scheduling of distributed generators in a microgrid considering various constraintss," in *Proc. IEEE Power Energy Soc. Gen. Meeting*, Jul. 2009, pp. 1–6.

[24] Y. Li and Y. W. Li, "Power management of inverter interfaced autonomous microgrid based on virtual frequency-voltage frame," *IEEE Trans. Smart Grid*, vol. 2, no. 1, pp. 30–40, Mar. 2012.

[25] T. Khalifa, K. Naik, and A. Nayak, "A survey of communication protocols for automatic meter reading applications," *IEEE Commun. Surveys Tuts.*, vol. 13, no. 2, pp. 168–182, 2nd Quart., 2011.

[26] D. Vyas and H. Pandya, "Advance metering infrastructure and DLMS/COSEM standards for smart grid," *Int. J. Eng. Res. Technol.*, Vol. 1, no. 10, pp. 1–5, Dec. 2012.

[27] M. A. Qureshi, I. Ahmad, and M. F. Munir, "Double integral sliding mode control of continuous gain four quadrant quasi-Z-source converter," *IEEE Access*, vol. 6, pp. 77785–77795, 2018.

[28] F. Blaabjerg, R. Teodorescu, Z. Chen, and M. Liserre, "Power converters and control of renewable energy systems," in *Proc. 6th Int. Conf. Power Electron*, Oct. 2004, Vol. 1, pp. 1–20.

[29] S. B. Kjaer, J. K. Pedersen, and F. Blaabjerg, "A review of single-phase grid-connected inverters for photovoltaic modules," *IEEE Trans. Ind. Appl.*, vol. 41, no. 5, pp. 1292–1306, Sep. 2005.

[30] V. Vorperian, "Simplified analysis of PWM converters using model of PWM switch. II. Discontinuous conduction mode," *IEEE Trans. Aerosp. Electron. Syst.*, vol. 26, no. 3, pp. 490–496, May 1990.

[31] J. Kim, J. Choi, and H. Hong, "Output LC filter design of voltage source inverter considering the performance of controller," in *Proc. PowerCon Int. Conf. Power Syst. Technol.*, vol. 3, Dec. 2000, pp. 1659–1664.

[32] M. Liserre, F. Blaabjerg, and S. Hansen, "Design and control of an LCL-filter-based three-phase active rectifier," *IEEE Trans. Ind. Appl.*, vol. 41, no. 5, pp. 1281–1291, Sep./Oct. 2005.

[33] V. Kaura and V. Blasko, "Operation of a phase locked loop system under distorted utility conditions," *IEEE Trans. Ind. Appl.*, vol. 33, no. 1, pp. 58–63, Jan./Feb. 1997.

[34] S. M. Silva, B. M. Lopes, B. J. C. Filho, R. P. Campana, and W. C. Bosventura, "Performance evaluation of PLL algorithms for single-phase grid-connected systems," in *Proc. IEEE Ind. Appl. Conf.*, vol. 4, Oct. 2004, pp. 2259–2263.

[35] Q.-C. Zhong and D. Boroyevich, "Structural resemblance between droop controllers and phase-locked loops," *IEEE Access*, vol. 4, pp. 5733–5741, 2016.

[36] W. Wenkai, N. Pongratananukul, Q. Weihong, K. Rustom, T. Kasparis, and I. Batarseh, "DSP-based multiple peak power tracking for expandable power system," in *Proc. IEEE 18th Annu. Appl. Power Electron. Conf. Expo.*, Feb. 2003, pp. 525–530.

[37] D. P. Hohm and M. E. Ropp, "Comparative study of maximum power point tracking algorithms using an experimental, programmable, maximum power point tracking test bed," in *Proc. IEEE 28th Conf. Rec. Photovoltaic Spec. Conf.*, Sep. 2000, pp. 1699–1702.

[38] F. Taeed and M. Nymand, "A novel high performance and robust digital peak current mode controller for DC-DC converters in CCM," in *Proc. IEEE 15th Workshop Control Model. Power Electron. (COMPEL)*, Santander, Spain, Jun. 2014, pp. 1–5.

[39] M. Á. A. Fong, J. J. R. Rivas, O. C. Castillo, R. O. Gonzalez, and J. C. T. Barrera, "Control of a boost converter to improve the performance of a photovoltaic system in a microgrid," in *Proc. Environ., Green Technol. Eng. Int. Conf. (EGTEIC)*, Nov./Oct. 2018, Vol. 2.

[40] V. Vásquez, L. M. Ortega, D. Romero, R. Ortega, O. Carranza, and J. J. Rodríguez, "Comparison of methods for controllers design of single phase inverter operating in island mode in a microgrid," *Rev. Renew. Sustain. Energy Rev.*, vol. 76, pp. 256–267, Sep. 2017.

[41] *IEEE Recommended Practice for Utility Interface of Photovoltaic (PV) Systems*, IEEE Standard 929, 2000.

[42] L. Li, C. Hu, J. Hu, and Y. Dong, "Islanding detection method for PV grid-connected inverter based on dynamic reactive power disturbance," in *Proc. IEEE 10th Conf. Ind. Electron. Appl. (ICIEA)*, Auckland, New Zealand, Jun. 2015, pp. 1471–1475.

[43] D. Xie, D. Zang, P. Gao, M. Xiang, and L. Yang, "Research on islanding detection technology for multi grid-connected inverters," in *Proc. IEEE 2nd Adv. Inf. Technol., Electron. Automat. Control Conf. (IAEAC)*, Chongqing, China, Mar. 2017, pp. 2505–2508.

[44] T. Thacker, F. Wang, and D. Boroyevich, "Islanding control of a distributed generation unit's power conversion system to the electric utility grid," in *Proc. IEEE 36th Power Electron. Spec. Conf. (PESC)*, Jun. 2005, pp. 210–216.

[45] W. Yao, M. Chen, J. Matas, J. M. Guerrero, and Z.-M. Qian, "Design and analysis of the droop control method for parallel inverters considering the impact of the complex impedance on the power sharing," *IEEE Trans. Ind. Electron.*, vol. 58, no. 2, pp. 576–588, Feb. 2011.

[46] J. M. Guerrero, N. Berbel, J. Matas, L. G. de Vicuna, and J. Miret, "Decentralized control for parallel operation of distributed generation inverters in microgrids using resistive output impedance," in *Proc. IEEE 32nd Annu. Conf. Industrial Electron.*, Nov. 2006, pp. 5149–5154.

[47] S. J. Chiang, C. Y. Yen, and K. T. Chang, "A multimodule parallelable series-connected PWM voltage regulator," *IEEE Trans. Ind. Electron.*, vol. 48, no. 3, pp. 506–516, Jun. 2001.

[48] H.-P. Glauser, M. Keller, A. Plüss, M. Schwab, and R. Scherwey, "New inverter module with digital control for parallel operation," in *Proc. IEEE TELESCON Conf.*, May 2000, pp. 265–269.

[49] Y. Shtessel, C. Edwards, L. Fridman, and A. Levant, *Sliding Mode Control and Observation*, 1st ed. Basel, Switzerland: Birkhäuser, 2015.

[50] R. Ortega, O. Carranza, J. C. Sosa, V. H. García, and N. Y. Ortega, "Application control configurations in a photovoltaic inverter operating in a microgrid," in *Proc. IEEE 41st Annu. Conf. Ind. Electron. Soc. (IECON)*, Nov. 2015, pp. 001014–001019.

[51] *PSIM 11.1 User's Guide*, Powersim, Rockville, MD, USA, Jul. 2018.

[52] C. Li, M. Savaghebi, J. C. Vasquez, and J. M. Guerrero, "Multiagent based distributed control for operation cost minimization of droop controlled AC microgrid using incremental cost consensus," in *Proc. 17th Eur. Conf. Power Electron. Appl. (EPE ECCE)*, Geneva, Switzerland, Sep. 2015, pp. 1–9.

[53] H. Han, Y. Liu, Y. Sun, M. Su, and J. M. Guerrero, "An improved droop control strategy for reactive power sharing in islanded microgrid," *IEEE Trans. Power Electron.*, vol. 30, no. 6, pp. 3133–3141, Jun. 2015.

RUBÉN ORTEGA received the B.Sc. degree in electrical engineering and the M.Sc. degree in systems engineering from the Instituto Politécnico Nacional, Ciudad de Mexico, Mexico, in 1999, and the D.E.A. degree in electrical engineering, computer, and electronic system from the Universidad de Oviedo, Oviedo, Spain, in 2009. He is currently pursuing the Ph.D. degree with the Universidad Politécnica de Valencia, Valencia, Spain. He has been a Professor with the Department of Computer Science and Engineering, Escuela Superior de Cómputo, Instituto Politécnico Nacional, since 1995. His main research interests include modeling and control of power converters applied to the distributed generation in microgrids, and digital signal processing.

OSCAR CARRANZA received the B.S. degree in communication and electronics engineering from the Instituto Politécnico Nacional, Ciudad de México, Mexico, in 1996, the M.Sc. degree in electronics engineering from the Instituto Politecnico Nacional, Ciudad de México, Mexico, in 1999, and the Ph.D. degree in electronics engineering from the Universidad Politécnica de Valencia, Valencia, Spain, in 2012. He has been a Professor with the Escuela Superior de Computo, Instituto Politecnico Nacional, since 1999. His main research fields include the modeling and control of power converters, power processing of renewable energy sources, and grid-connected converters for distributed power.

JAIME JOSÉ RODRÍGUEZ received the B.S. degree from the Universidad Central de Las Villas (UCLV), Santa Clara, Cuba, in 1980, and the M.S. and Ph.D. degrees in electrical engineering from the Moscow Power Engineering Institute, Moscow, Russia, in 1987 and 1991, respectively. From 1980 to 1994, he was an Associate Professor at UCLV. Since 1996, he has been with the Instituto Politecnico Nacional, Ciudad de México, Mexico, where he is currently a Titular Professor and a Researcher in power electronics and AC control drives. Dr. Rodríguez is currently a member of the National System of Researchers of Mexico.

VICTOR H. GARCÍA received the Engineering degree in computation systems and the M.Sc. degree from the Instituto Politecnico Nacional, Ciudad de México, Mexico, in 1999 and 2006, respectively. He has been a Professor of computer architecture with the Escuela Superior de Computo, Instituto Politecnico Nacional, since 2004. His current research interest include computer architecture, signal and image processing, and embedded systems.

JULIO C. SOSA received the Engineering degree in electrónic engineering from the Instituto Tecnológico de Lazaro, Mexico, in 1997, the M.Sc. degree in electrical engineering from CINVESTAV-IPN, Mexico, in 2000, and the Ph.D. degree in technology of information and computation from the University of Valencia, Spain, in 2007. He is currently a Professor of computer architecture with the Escuela Superior de Computo, Instituto Politecnico Nacional, Mexico, since 1997. Her current research interests are reconfigurable systems, hardware architectures for motion estimation, and educational computing.

JOSÉ M. ALVARADO received the B.Sc. degree in mechatronics engineering and the M.Sc. degree in electrical engineering from the Instituto Politécnico Nacional, Mexico, in 2011 and 2017, respectively, where he is currently pursuing the Ph.D. degree in energy. He has extensive experience in the industry and his areas of interest are: control of electronic converters, control of electric motors, power electronics, and embedded systems.